Jurnal Mekanova : Mekanikal, Inovasi dan Teknologi
Vol 12 No. 2, Oktober 2026
P-ISSN : 2477-5029
E-ISSN : 2502-0498

Preliminary Design and Machine-Learning Surrogate Modelling of Training-Glider Flight Performance

T. A. Sukhairi*[1], M. Nofian Sukmana[2], Ikramullah Muhammad[1], Syahrul Fathi[3], Mufti[4]
[1]Department of Mechanical and Industrial Engineering, Universitas Syiah Kuala, Jl. Tgk. Syech Abdurrauf No. 7, Darussalam, Banda Aceh 23111, Indonesia
[2]Aerospace Engineering, Institut Teknologi Dirgantara Adisutjipto, Yogyakarta, Indonesia
[3]Department of Mechanical Engineering, Universitas Teuku Umar, Meulaboh, Indonesia
[4]Aerospace Engineering, Universitas Dirgantara Marsekal Suryadarma, Jakarta, Indonesia
e-mail: *[1]teuku.arriessa@usk.ac.id

Abstrak

Pesawat layang latih merupakan wahana dasar pendidikan penerbang, namun kapabilitas perancangannya di Indonesia masih terbatas. Penelitian ini menyusun rancangan awal pesawat layang latih satu kursi untuk tahap terbang solo awal dan mengembangkan model surrogate berbasis pembelajaran mesin untuk prestasi terbang luncur tunak. Rancangan mengikuti metode Raymer dengan airfoil NACA 6409 yang dianalisis menggunakan NeuralFoil dan massa lepas landas 420,3 kg sesuai beban awak CS-22. Efisiensi aerodinamika maksimum adalah 21,67 dan kecepatan stall 20,56 m/s. Dari ketinggian 600 m di udara tenang, jangkauan dan ketahanan terbang adalah 13,0 km dan 10,4 menit pada kecepatan luncur terbaik, atau 12,8 km dan 9,5 menit dengan batas 1,1 kali kecepatan stall; target 20 menit tidak tercapai dan memerlukan ketinggian lepas sekitar 1268 m atau bantuan termal. Lima model regresi dilatih pada 2000 sampel Latin Hypercube yang dibangkitkan dari persamaan analitik deterministik, sehingga akurasinya mengukur ketelitian aproksimasi, bukan validasi fisik. Gaussian Process Regression paling akurat (MAPE validasi silang 10-fold 0,005%, galat persentil-95 di bawah 0,08%) dengan selang prediksi yang konservatif. Indeks Sobol' menunjukkan koefisien drag parasit dan rasio aspek mengendalikan efisiensi, sedangkan beban sayap dan koefisien gaya angkat maksimum mengendalikan kecepatan stall.

Kata kunci*—pesawat layang, rancangan awal, prestasi terbang, model surrogate, analisis sensitivitas*

Abstract

Training gliders are the entry platform of pilot education, yet domestic design capability for this class in Indonesia remains limited. This study develops the preliminary design of a single-seat glider for the early solo phase of training and a machine-learning (ML) surrogate of its steady-glide performance. The design follows Raymer's method with a NACA 6409 section analysed with NeuralFoil and a take-off mass of 420.3 kg based on the CS-22 occupant allowance. The maximum aerodynamic efficiency is 21.67 and the stall speed 20.56 m/s. From a 600 m release in still air, the range and endurance are 13.0 km and 10.4 min at the theoretical best-glide speed, or 12.8 km and 9.5 min with a 1.1 stall-speed margin; the 20 min requirement is not met and needs a release height of about 1268 m or thermal lift. Five regressors were trained on 2000 Latin Hypercube samples generated by deterministic analytical equations, so their accuracy measures approximation fidelity rather than physical validation. Gaussian Process Regression was the most accurate (10-fold cross-validated MAPE 0.005%, 95th-percentile error below 0.08%) and its prediction intervals were conservative. Sobol' indices show that parasite drag and aspect ratio govern aerodynamic efficiency, while wing loading and maximum lift coefficient govern stall speed.

Keywords*—glider, preliminary design, flight performance, surrogate modelling, sensitivity analysis*

1. INTRODUCTION

Gliders, or sailplanes, are heavier-than-air aircraft whose flight is sustained entirely by aerodynamic efficiency and gravitational potential energy. As trainers they develop energy management, airspeed discipline and situational awareness without the workload of an engine [1]. In Indonesia, gliding is organised by the Federasi Aero Sport Indonesia (FASI), and the fleet still relies largely on imported, ageing types; national efforts such as the GL-1 sailplane programme have only recently begun to address domestic design capability [2].

Preliminary design is the stage in which the configuration is frozen and the aerodynamic, weight and performance estimates become accurate enough to commit to detailed design [3]. For an unpowered aircraft the entire flight envelope follows from the drag polar and the wing loading fixed at this stage [1,4]. Modern sailplane research has pushed laminar-flow airfoils and planforms to glide ratios above 40 [5], and early sailplane studies already used parametric sweeps of wing area, taper and twist to balance performance against handling and simplicity [6].

Machine learning (ML) has become an established tool in aerodynamics, mainly for surrogate modelling and design-space exploration [7-9]. Most work operates at the airfoil or flow-field level [10-12]. At the aircraft level, Liem et al. [13] built kriging and mixture-of-experts surrogates of high-fidelity aerodynamic coefficients and obtained range errors below 2% in mission analysis; Rao and Chimata [14] trained tree, nearest-neighbour and neural-network surrogates on 47,000 physics-based eVTOL simulations and reported range and endurance errors below 2% on hold-out data, without uncertainty quantification; Tfaily et al. [15] used transfer learning with mixtures of experts to reduce surrogate error in industrial conceptual aircraft design; and Opgenoord et al. [16] applied variance-based sensitivity analysis to the conceptual design of a transport aircraft. These studies report point accuracy on hold-out data but rarely assess whether the predictive uncertainty is calibrated or whether the surrogate preserves the global sensitivity structure of the underlying model, and none addresses a training glider, whose endurance is governed by the interaction between the drag polar and the stall margin.

This paper addresses that gap for a single-seat training glider. The configuration, geometry and empty mass are taken from an earlier study by the authors [17], which estimated the performance from section-level lift-to-drag ratios. The new elements are: (i) a revised take-off mass based on the CS-22 occupant allowance [18]; (ii) an independent NeuralFoil analysis of the wing section; (iii) a performance model based on the whole-aircraft drag polar with an explicit stall margin, which distinguishes theoretical best-glide from operationally constrained performance; (iv) a 2000-sample Latin Hypercube dataset and a 10-fold cross-validated comparison of five regressors, including fold variability, residuals near the stall-margin switch and calibration of the Gaussian-process prediction intervals; and (v) Sobol' indices computed from both the analytical model and the surrogate, together with a design map and an assumption-sensitivity study of the release height needed for 20 min endurance. Because the data generator is analytical, the surrogate error can be measured exactly; the study is therefore a controlled benchmark of the workflow before it is applied to CFD, wind-tunnel or flight-test data, for which no closed form exists.

2. RESEARCH METHOD

The study has two linked stages (Figure 1). Stage 1 establishes the preliminary design following Raymer [3], yielding the configuration, mass, geometry and a closed-form steady-glide performance model. Stage 2 uses this model as a data generator for ML surrogates, which are cross-validated, checked at the design point and interpreted with Sobol' indices. Structural sizing, stability, control and handling qualities are outside the scope of this work.

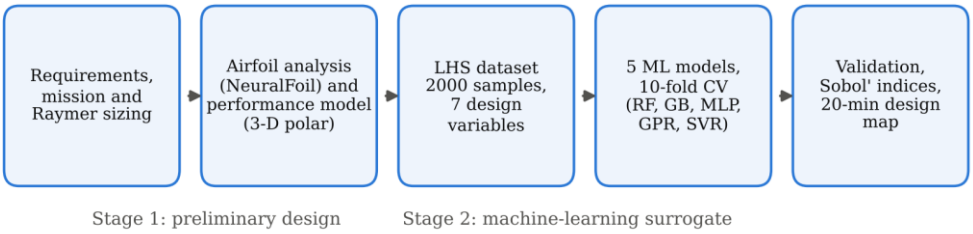


Figure 1 Research workflow

2.1 Design requirements, mission and mass

The glider is intended for the early solo phase of training, after dual instruction in a two-seat trainer, with a target of 20 min of flight after aerotow release at about 600 m above ground. A single-seat layout keeps the aircraft light and inexpensive and reproduces the role of the single-seat types that still form the Indonesian club fleet [2]. The mission comprises (a) taxi, (b) aerotow take-off, (c) climb on tow, (d) release, gliding and observation, (e) descent, (f) final approach and landing, and (g) landing roll (Figure 2). The empty mass is 310.3 kg [17]. The useful load is set to 110 kg for the occupant and parachute, the value that CS 22.25 requires as the minimum allowance for a single-seat sailplane [18]; no water ballast or additional equipment is carried. The design take-off mass is therefore m_0 = 420.3 kg and the wing loading 40.0 kg/m^2. The effect of a lighter or ballasted pilot is examined in Section 3.6.

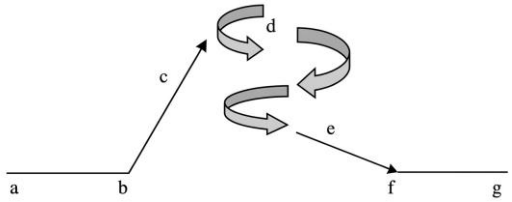


Figure 2 Sizing mission profile: (a) taxi, (b) aerotow take-off, (c) climb, (d) gliding and observation, (e) descent, (f) final approach and landing, (g) landing roll

2.2 Geometry sizing and design assumptions

The fuselage length follows Raymer's statistical relation [3]

$$l = a\, m_0^{C} \tag{1}$$

with m_0 in kg and l in m. The tail moment arm is 65% of the fuselage length, typical of sailplanes, and the tail areas follow the tail-volume method [3]:

$$L = 0.65\, l, \qquad S_{HT} = \frac{c_{HT}\,\bar{c}\,S}{L_{HT}}, \qquad S_{VT} = \frac{c_{VT}\,b\,S}{L_{VT}} \tag{2}$$

where S, b and $\bar{c}$ are the wing area, span and mean aerodynamic chord. For a trapezoidal wing with taper ratio λ the chords are

$$c_r = \frac{2S}{b(1+\lambda)}, \qquad c_t = \lambda c_r, \qquad \bar{c} = \frac{2}{3} c_r \frac{1+\lambda+\lambda^2}{1+\lambda} \tag{3}$$

With b = 15 m, S = 10.498 m^2 and λ = 0.5, the aspect ratio is $AR = b^2/S$ = 21.4. The fuselage length of 5.70 m was retained from the earlier configuration [17]; Eq. (1) with the homebuilt-class coefficients a = 1.35 and C = 0.23 reproduces it for the original mass estimate, and the revised mass would shorten it by only 0.3 m. The geometry is listed in Table 1 and the main

assumptions, their basis and plausible alternatives in Table 2. The parasite drag coefficient was not derived from a component build-up; it is a conservative assumption checked against the equivalent skin-friction method [3]. The estimated wetted area is about 31 m^2 (wing 20.4, tails 3.8 and fuselage 6.7 m^2), i.e. $S_{wet}/S \approx 2.95$. With the equivalent skin-friction coefficient of a light single-engine aircraft, C_{fe} = 0.0055, this gives $C_{D0} \approx 0.016$, whereas the adopted value 0.034 corresponds to $C_{fe} \approx 0.0115$. The baseline is therefore an upper bound that allows for fabric covering, a fixed wheel, canopy gaps and non-laminar flow, and the range 0.012-0.050 is explored in the parametric study.

Table 1 Geometry and configuration of the training glider

Parameter	Value
Fuselage length / diameter	5.70 / 0.50 m
Tail moment arm, L	3.70 m
Wing span / area	15.00 m / 10.498 m^2
Aspect ratio / taper ratio	21.4 / 0.5
Root / tip / mean chord	0.933 / 0.466 / 0.725 m
Horizontal / vertical tail area	1.028 / 0.851 m^2
Empty / take-off mass	310.3 / 420.3 kg
Wing loading, m_0/S	40.0 kg/m^2
Wing / tail airfoil	NACA 6409 / NACA 0012
Configuration	High wing, T-tail, tail wheel, single seat

Table 2 Main design assumptions, basis and alternatives

Item	Value	Basis	Alternatives / treatment
Wing section	NACA 6409	High camber gives $c_{l,max} \approx$ 1.5 and a gentle stall at low Re [19]	Wortmann or NACA 6-series laminar sections (lower drag, sharper stall)
Fuselage regression	a = 1.35, C = 0.23	Homebuilt class [3]; compact, low-cost fuselage	Sailplane class (a = 0.383, C = 0.48): about 7 m, longer tail arm
Tail volumes	c_{HT} = 0.50, c_{VT} = 0.02	Raymer's sailplane values [3]	Stability-based sizing in detailed design
Oswald factor	e = 0.95	High-AR, untwisted, tapered wing [20]	0.85-0.98 (sampled)
Parasite drag	C_{D0} = 0.034	Conservative upper bound; C_{fe} method gives ≈ 0.016	0.012-0.050 (sampled)
Aircraft $C_{L,max}$	1.517	≈ 0.9 × section $c_{l,max}$ at flight Re (Section 3.1)	1.2-1.8 (sampled)
Air density	1.225 kg/m^3	Sea level; simple and conservative for sink rate	ISA and ISA + 15 K (Section 3.6)
Stall margin	$V \geq 1.1V_s$	Minimum practical margin for steady glide	Best glide without margin also reported

2.3 Airfoil analysis

The NACA 6409 section (6% camber at 40% chord, 9% thickness [19]) was analysed with NeuralFoil (version 0.3.3, xlarge model), a physics-informed neural network trained on XFOIL [21] solutions [12], at the flight Reynolds number at best-glide speed, Re = 1.04e+06 (sea level, $\bar{c}$ = 0.725 m), and at $Re = 4.57\times10^5$ for comparison with panel-method (DesignFOIL) data for the same section [17].

2.4 Flight performance model

Steady, trimmed gliding flight with a parabolic drag polar is assumed [3,4]. The mass is denoted m (kg) and the weight mg (N). The induced-drag factor follows from the Oswald factor e:

$$C_D = C_{D0} + k\,C_L^2, \qquad k = \frac{1}{\pi AR\,e} \tag{4}$$

The maximum aerodynamic efficiency and the corresponding lift coefficient are

$$E_m = \left(\frac{L}{D}\right)_{\max} = \frac{1}{2\sqrt{k\,C_{D0}}}, \qquad C_L^* = \sqrt{\frac{C_{D0}}{k}} \tag{5}$$

The stall speed and the minimum-drag (best-glide) speed are

$$V_s = \sqrt{\frac{2mg}{\rho S C_{L,\max}}}, \qquad V_{Dmin} = \sqrt{\frac{2mg}{\rho S}}\left(\frac{k}{C_{D0}}\right)^{1/4} \tag{6}$$

and the minimum glide angle is $\gamma_{\min} = \arctan(1/E_m)$. For a given lift coefficient the sink rate and the still-air range and endurance from release height h_0 are

$$w = V\frac{C_D}{C_L}, \qquad R = h_0\frac{C_L}{C_D}, \qquad t = \frac{h_0}{w} \tag{7}$$

where C_L/C_D is the whole-aircraft ratio from Eq. (4), not the section ratio c_l/c_d. Two operating conditions are distinguished. The theoretical best-glide condition uses C_L^* without restriction. The operational condition limits the lift coefficient to $C_{L,op} = C_{L,max}/1.1^2$ (i.e. $V \geq 1.1V_s$); range is then evaluated at $C_L = \min(C_L^*, C_{L,op})$ and the maximum endurance at the minimum-sink condition

$$C_{L,ms} = \min\left(\sqrt{\frac{3C_{D0}}{k}},\ C_{L,op}\right) \tag{8}$$

Unless stated otherwise, R and t refer to the operational condition. The baseline uses $C_{L,max} = 1.517$, $C_{D0} = 0.034$, $e = 0.95$ and $\rho = 1.225$ kg/m^3. The landing ground roll follows Raymer's integrated equation for zero thrust [3], with touchdown at $1.15V_s$, 1 s of free roll, braking friction $\mu = 0.3$ on grass and a ground-attitude lift coefficient $C_{L,g} = 0.7$:

$$s_g = \frac{1}{2gK_A}\ln\left(\frac{K_T}{K_T + K_A V_{TD}^2}\right), \quad K_T = -\mu, \quad K_A = \frac{\rho}{2mg/S}\left(\mu C_{L,g} - C_{D0} - kC_{L,g}^2\right) \tag{9}$$

To quantify the effect of the sea-level density assumption, the release height h_{req} for a target endurance t^* was also computed in the ISA atmosphere (and ISA + 15 K), with the sink rate at fixed C_L scaled by $(\rho_0/\rho(h))^{1/2}$:

$$t^* = \int_0^{h_{req}} \frac{dh}{w_0\sqrt{\rho_0/\rho(h)}} \tag{10}$$

2.5 Parametric dataset

Seven design variables were varied: AR, S, m, $C_{L,max}$, C_{D0}, e and h_0 (Table 3). A total of 2000 samples were drawn by Latin Hypercube Sampling (LHS) [22] (SciPy, seed 42). For every sample the six targets V_s, E_m, V_{Dmin}, γ_{min}, R and t were computed from Eqs. (4)-(8). Four targets are smooth functions of the inputs, whereas R and t contain a non-differentiable switch where the stall margin becomes active. Three engineered features that appear in the governing equations, wing loading m/S, span $b = (AR \cdot S)^{1/2}$ and k, were added to the seven raw inputs. The baseline design is not part of the dataset.

Table 3 Design space of the parametric dataset (n = 2000, LHS)

Design variable	Min	Max	Baseline	Unit
Aspect ratio, AR	15	30	21.4	-
Wing area, S	8.0	14.0	10.498	m^2
Mass, m	400	650	420.3	kg
Max lift coefficient, $C_{L,max}$	1.2	1.8	1.517	-
Parasite drag coefficient, C_{D0}	0.012	0.050	0.034	-
Oswald factor, e	0.85	0.98	0.95	-
Release height, h_0	500	2000	600	m

2.6 Machine learning models and reproducibility

Five regressors were compared: Random Forest (RF; 200 trees, maximum depth 20, minimum leaf size 2) [23]; Gradient Boosting (GB; 300 trees, learning rate 0.08, depth 5, one model per target) [24]; a Multilayer Perceptron (MLP; 128-64-32 ReLU neurons, Adam, learning rate 10^{-3}, early stopping on a 10% validation split, patience 50); Gaussian Process Regression (GPR; constant × anisotropic Matern 5/2 kernel plus white noise, one model per target) [25]; and Support Vector Regression (SVR; RBF kernel, $\varepsilon = 0.01$) [26]. The RF, GB and MLP settings were fixed a priori; all stochastic components used seed 42. For SVR, $C \in \{1, 10, 100, 1000\}$ and the kernel width $\gamma \in \{\text{scale}, 0.05, 0.1\}$ were selected by an inner 3-fold grid search. For GPR, the length scales (bounds 10^{-2}-10^{3}) and noise level (bounds 10^{-10}-10^{-1}) were obtained by maximising the log-marginal likelihood with L-BFGS-B (one restart) on a random 500-point subset of each training fold, after which the process was conditioned on the full fold.

All models were evaluated by 10-fold cross-validation (shuffled, seed 42) on the 2000 samples. Input and output standardisation, the SVR grid search and the GPR hyperparameter optimisation were embedded in one pipeline and fitted only on the training part of each fold, so no information from the test fold entered the training. The metrics are the coefficient of determination, the normalised RMSE (RMSE divided by the target range), the mean absolute percentage error and its 95th percentile:

$$R^2 = 1 - \frac{\sum_i (y_i - \hat{y}_i)^2}{\sum_i (y_i - \bar{y})^2}, \qquad \text{MAPE} = \frac{100\%}{n} \sum_i \left| \frac{y_i - \hat{y}_i}{y_i} \right| \tag{11}$$

The calibration of the GPR predictive distribution $N(\mu_i, \sigma_i^2)$ was assessed by the empirical coverage of the central intervals $\mu_i \pm z_p \sigma_i$ for nominal levels p = 0.50-0.99, using out-of-fold predictions. The computations used Python 3.13, NumPy 2.5, SciPy 1.18, scikit-learn 1.9.1 [27], SALib 1.6.0 [28] and NeuralFoil 0.3.3; the scripts and dataset are available from the corresponding author.

2.7 Global sensitivity analysis

Variance-based Sobol' indices [29] were used to rank the seven raw design variables. The total-order index of variable X_i,

$$S_{T,i} = \frac{\mathbb{E}_{\mathbf{X}_{\sim i}}\left[\text{Var}_{X_i}(Y|\mathbf{X}_{\sim i})\right]}{\text{Var}(Y)} \tag{12}$$

measures the share of output variance caused by X_i including its interactions. The indices were estimated with the Saltelli scheme [30] in SALib using 4096 base samples (36,864 evaluations), once with the analytical model and once with the trained surrogate.

3. RESULTS AND DISCUSSION

3.1 Airfoil characteristics

Figure 3 shows the NeuralFoil results. At the flight Reynolds number the section reaches $c_{l,max}$ = 1.69 near 14° and a maximum c_l/c_d of about 154. At Re = 4.57×10^5 the maximum lift coefficient falls to 1.545, in close agreement with the panel-method data (1.517, mean absolute difference in c_l of 0.046). Because a finite wing typically reaches about 90% of the section maximum [3], the aircraft maximum lift coefficient was set to $C_{L,max}$ = 1.517, slightly below 0.9 × 1.69 ≈ 1.52 and equal to the low-Re section maximum, which is conservative for stall speed. Both data sets are numerical; no wind-tunnel validation of the section or wing was performed.

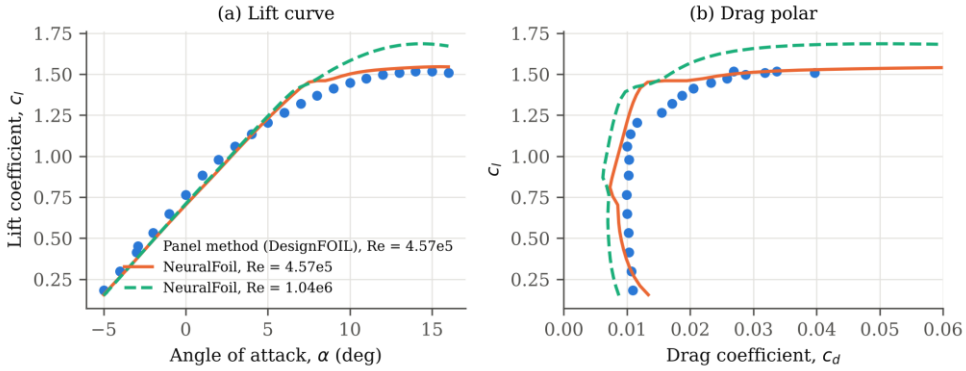


Figure 3 NACA 6409 section characteristics from NeuralFoil at the flight and a lower Reynolds number, with panel-method data at the lower Reynolds number

3.2 Preliminary design performance

Table 4 lists the baseline performance for both operating conditions. With k = 0.0157 the maximum aerodynamic efficiency is 21.67 at C_L^* = 1.474, and the stall speed is 20.56 m/s. At the theoretical best-glide speed (20.86 m/s) the sink rate is 0.962 m/s, giving 13.0 km and 10.4 min from 600 m. This speed is only 1.5% above the stall speed, so in practice the glider is flown at 1.1V_s = 22.6 m/s, where the range is 12.83 km and the endurance 9.46 min. The baseline therefore does not meet the 20 min requirement from 600 m in still air; it needs a release height of about 1268 m, or thermal lift, which is the normal operating mode of a glider. The landing ground run with braking is about 154 m, compatible with typical grass gliding strips.

Table 4 Baseline flight performance (sea-level density, m_0 = 420.3 kg)

Quantity	**Best glide (no margin)**	**Operational ($V \geq 1.1V_s$)**
Induced-drag factor, k	0.0157	-
Maximum aerodynamic efficiency, E_m	21.67	-
Stall speed, V_s	20.56 m/s	-
Lift coefficient	1.474	1.254
Flight speed	20.86 m/s	22.61 m/s
Glide ratio / glide angle	21.67 / 2.64°	21.39 / 2.68°
Sink rate	0.962 m/s	1.057 m/s
Range from 600 m	13.00 km	12.83 km
Endurance from 600 m	10.39 min	9.46 min
Release height for 20 min	1155 m	1268 m
Landing distance (μ = 0.3)	154 m	-

Figure 4 shows the whole-aircraft drag polar and the speed polar. The optimum lift coefficient lies only 3% below $C_{L,max}$ because of the conservative parasite drag (C_{D0} = 0.034) relative to the induced drag of the high-aspect-ratio wing. Because $C_{L,ms} = (3C_{D0}/k)^{1/2}$ = 2.55 exceeds $C_{L,max}$, the minimum-sink point is not attainable and endurance is always limited by the stall margin. For a trainer, where students fly slightly fast, this identifies parasite drag as the first target for design iteration, which the analysis below quantifies.

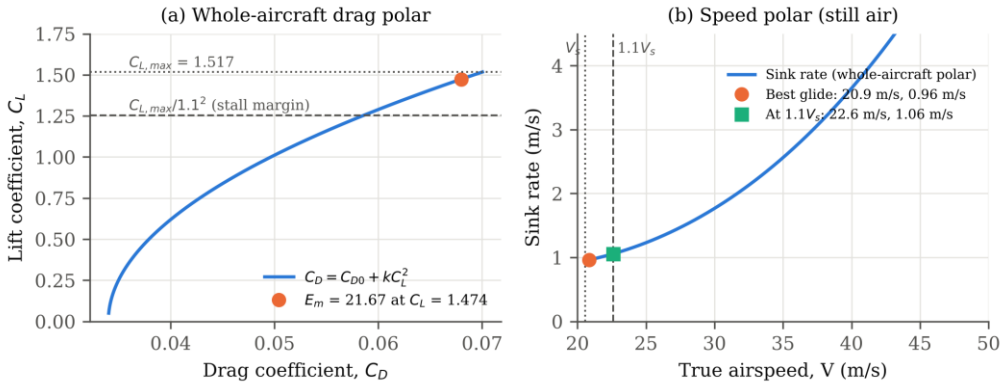


Figure 4 (a) Whole-aircraft drag polar and (b) still-air speed polar of the baseline design

3.3 Surrogate approximation accuracy

Table 5 Ten-fold cross-validation results averaged over the six targets (MAPE as mean ± standard deviation across folds)

Model	Mean R^2	Mean NRMSE (%)	MAPE (%)	Max P95 error (%)	Fit time (s)
Random Forest (RF)	0.948154	4.057	4.662 ± 0.217	26.541	10
Gradient Boosting (GB)	0.995060	1.150	1.389 ± 0.040	9.517	150
Multilayer Perceptron (MLP)	0.997999	0.822	1.013 ± 0.083	5.405	27
Gaussian Process Regression (GPR)	1.000000	0.007	0.005 ± 0.001	0.075	1153
Support Vector Regression (SVR)	0.999631	0.348	0.346 ± 0.030	1.904	1327

Table 6 Per-target 95th-percentile absolute percentage error (%) from 10-fold cross-validation

Model	V_s	E_m	V_{Dmin}	γ_{min}	R	t
RF	8.27	7.83	6.26	7.64	24.8	26.5
GB	0.926	1.45	2.31	1.55	5.61	9.52
MLP	0.933	2.13	1.2	1.77	5.41	5.1
GPR	8.03e-05	0.000379	0.00149	0.0002	0.0376	0.0753
SVR	0.307	1.05	0.503	0.623	1.9	1.83

Tables 5-6 and Figure 5 summarise the cross-validated accuracy. Because the data were generated by deterministic, smooth equations without noise, these figures measure how

faithfully each model approximates its analytical generator, not the physical accuracy of the performance model. Gaussian Process Regression is the most accurate (mean MAPE 0.0051%; 95th-percentile error below 0.075% for every target), followed by SVR (0.35%), the MLP (1.01%), GB (1.39%) and RF (4.66%). The fold-to-fold standard deviation of the MAPE is less than 10% of its mean for all models (Table 5), so the ranking does not depend on the partition. A stationary Gaussian process with automatic relevance determination interpolates the smooth power-law relations almost perfectly from 1800 points, whereas tree ensembles approximate them with piecewise-constant steps; RF is the weakest, particularly for the stall speed (R^2 = 0.885), whose dependence on m/S and $C_{L,max}$ must be represented by many axis-aligned splits. For every model the range and endurance are the most difficult targets, because they depend multiplicatively on h_0 and contain the stall-margin switch.

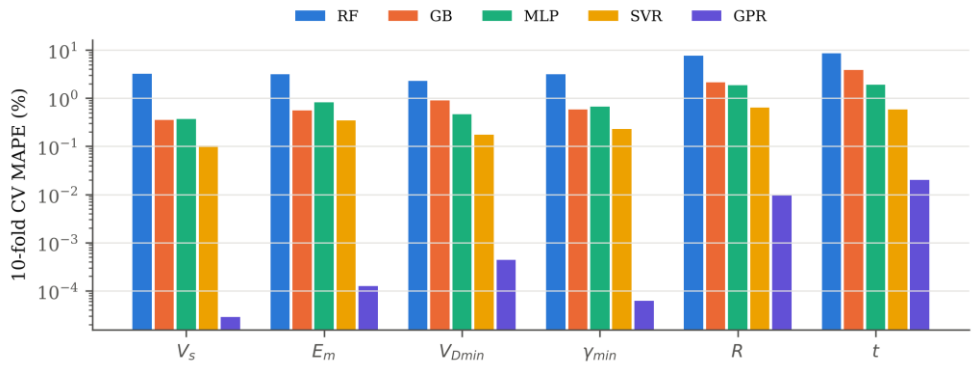


Figure 5 Ten-fold cross-validated MAPE of the five models for each target (logarithmic scale)

3.4 Residuals near the stall-margin switch and uncertainty calibration

The stall margin is active for 65% of the samples for range and 99.5% for endurance. Figure 6a plots the GPR out-of-fold error against the ratio of the unconstrained to the operational lift coefficient, which equals one at the switch. Within ±5% of the switch the GPR error rises from 0.0085% to 0.0184% for range and from 0.019% to 0.145% for endurance, confirming that the non-differentiable switch is the dominant source of surrogate error, although the largest single error remains 1.16%. For the other models the increase near the switch is at most about a factor of two (SVR, endurance: 0.58% to 1.11%), because their errors elsewhere are already two to four orders of magnitude larger than those of GPR.

Figure 6b compares the nominal and empirical coverage of the GPR prediction intervals. The intervals are conservative: the nominal 95% intervals contain 98.2-100.0% of the out-of-fold observations and the nominal 50% intervals 86-99%, and the standard deviation of the standardised residuals is 0.15-0.61 instead of 1, i.e. the predicted standard deviations are about 1.6 to 6.6 times larger than the actual errors. The over-dispersion is largest for the smooth targets and smallest for range and endurance, where the errors near the switch are larger. The intervals can therefore be used as safe upper bounds on the approximation error, but they are not sharp; recalibration (e.g. variance scaling on a validation set) would be needed before using them for probabilistic design. This assessment applies to analytical data; the behaviour with noisy CFD or test data remains to be shown.

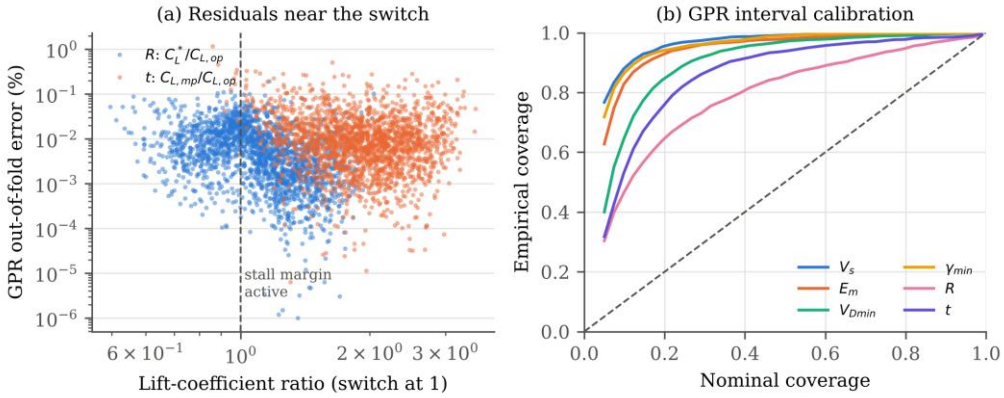


Figure 6 (a) GPR out-of-fold errors of range and endurance versus distance to the stall-margin switch; (b) calibration of the GPR prediction intervals

The cost of this accuracy is computational. GPR and SVR required about 19 and 22 min for the ten folds on a two-core machine, against seconds for RF and the MLP, and GPR is the slowest predictor (394 µs per design, against 0.06 µs for the closed-form equations). For the present analytical model the surrogate therefore offers no speed advantage; the demonstrated benefits are the quantified approximation error, conservative error bounds and the preserved sensitivity structure, whereas acceleration of expensive CFD-based evaluations is a potential future application [31,32].

3.5 Design-point check

Table 7 Prediction of the baseline design by the GPR surrogate trained on the 2000 samples

Target	Analytical	GPR	Error (%)
V_s (m/s)	20.5561	20.5561	2.94e-06
E_m (-)	21.6708	21.6708	2.85e-05
V_{Dmin} (m/s)	20.8565	20.8565	1.65e-05
γ_{min} (deg)	2.6420	2.6420	1.86e-05
R (km)	12.8345	12.8332	9.88e-03
t (min)	9.4601	9.4613	1.29e-02

The baseline design, which is not part of the dataset, was predicted by every final model (Table 7). The largest GPR error is 0.013%, whereas the maximum errors of SVR, MLP, GB and RF are 0.39%, 2.35%, 3.63% and 7.64%. This check verifies approximation fidelity only: the surrogate reproduces its generator, including any error in the assumptions of Table 2, so it does not validate the aircraft performance itself.

3.6 Sensitivity analysis and design implications

Figure 7 shows the total-order Sobol' indices of the seven design variables. The indices from the surrogate agree with those of the analytical model within 1.2e-04 for every target, so the surrogate preserves the sensitivity structure. The stall speed is governed by the wing area (S_T = 0.44), the mass (0.33) and $C_{L,max}$ (0.23). The maximum aerodynamic efficiency and the glide angle are dominated by the parasite drag coefficient (S_T = 0.81 and 0.77), followed by aspect ratio (0.19 and 0.23); the Oswald factor is unimportant within its range (0.008). Range and endurance are controlled mainly by the release height (S_T = 0.68 and 0.64) and secondly by C_{D0} (0.31 and 0.26). Within the aircraft itself, parasite drag is therefore the most effective design lever, consistent with sailplane practice [1,5].

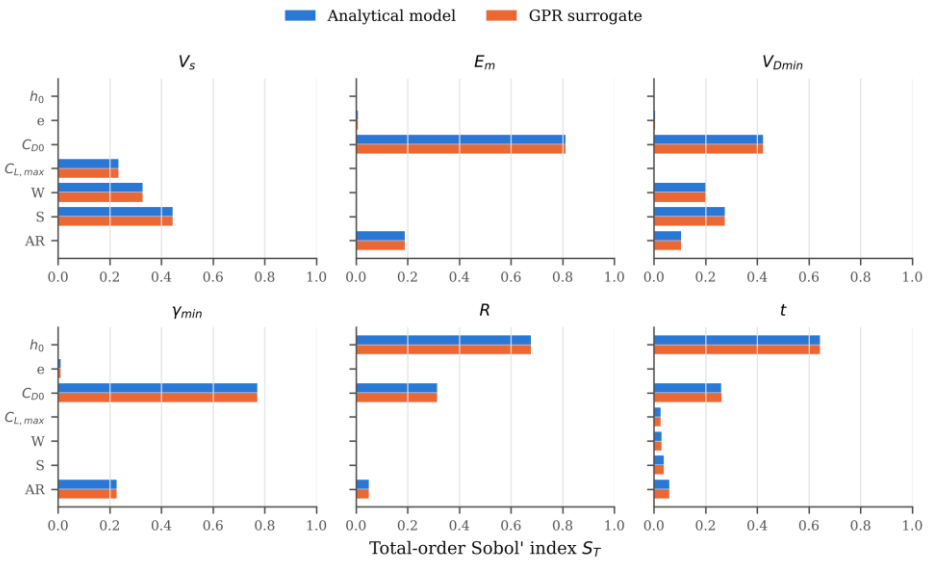


Figure 7 Total-order Sobol' indices of the design variables computed with the analytical model and with the GPR surrogate

Table 8 quantifies how the release height required for 20 min depends on the assumptions. Using the ISA atmosphere instead of constant sea-level density changes it from 1268 m to 1309 m, and a tropical day (ISA + 15 K) to 1344 m. A ±20% change in C_{D0} moves it between 1121 and 1416 m, and the extreme combinations span 1184-1506 m. In every case the still-air endurance from 600 m stays between 8.1 and 10.7 min.

Table 8 Sensitivity of the operational sink rate, the endurance from 600 m and the release height required for 20 min

Case	**Sink rate (m/s)**	***t* from 600 m (min)**	**h_{req} (m)**
Baseline (sea-level density)	1.057	9.5	1268
ISA standard atmosphere	1.057	9.3	1309
ISA + 15 K (tropical day)	1.057	9.1	1344
C_{D0} - 20% (0.0272)	0.934	10.7	1121
C_{D0} + 20% (0.0408)	1.180	8.5	1416
e = 0.85	1.109	9.0	1331
e = 0.98	1.043	9.6	1252
$C_{L,max}$ - 10% (1.365)	1.139	8.8	1367
$C_{L,max}$ + 10% (1.669)	0.997	10.0	1196
Mass 400 kg (light pilot)	1.031	9.7	1237
Mass 460 kg (+40 kg ballast)	1.106	9.0	1327
C_{D0} - 20% and ISA + 15 K	0.934	10.3	1184
C_{D0} + 20% and ISA + 15 K	1.180	8.1	1506

Finally, the surrogate was used to map the release height required for 20 min over the AR-C_{D0} plane at the baseline mass, wing area and $C_{L,max}$ (Figure 8); surrogate and analytical contours agree within 0.010% on average. Reducing C_{D0} from 0.034 to 0.016, the value given by the skin-friction estimate, lowers the requirement to about 872 m, and the most favourable corner of the map (AR = 30, C_{D0} = 0.012) still needs about 640 m. Across the 2000-sample dataset, 1 design reach 20 min from 600 m. Within the investigated assumptions and sampled domain, the 20 min still-air requirement from 600 m is therefore difficult to achieve; it is better

expressed as a release height of about 1 km for a low-drag airframe, or as a soaring task that relies on thermal lift.

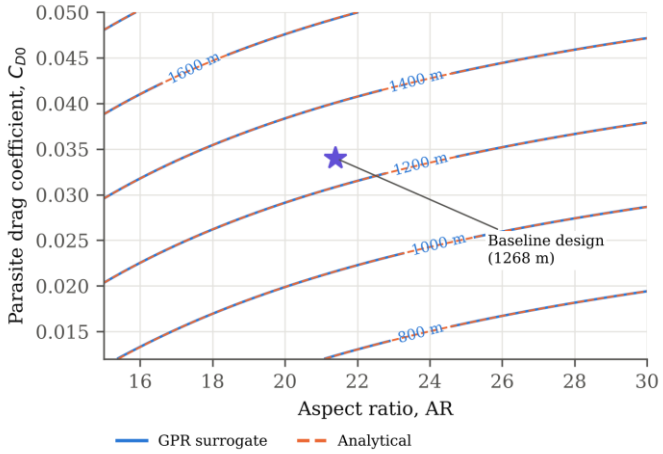


Figure 8 Release height required for 20 min still-air endurance as a function of aspect ratio and parasite drag coefficient (baseline m, S, $C_{L,max}$)

4. CONCLUSION

A preliminary design of a single-seat training glider was developed and its steady-glide performance was emulated with ML surrogates and analysed with Sobol' indices. The main conclusions are:

1. The design (m_0 = 420.3 kg, b = 15 m, AR = 21.4, NACA 6409 wing, T-tail) has a stall speed of 20.56 m/s and a maximum aerodynamic efficiency of 21.67. Its theoretical best-glide speed (20.86 m/s) leaves almost no stall margin.
2. From 600 m in still air the endurance is 10.4 min at best glide and 9.5 min with a $1.1V_s$ margin (range 13.0 and 12.8 km). The baseline does not meet the 20 min requirement; it needs a release height of about 1268 m (ISA 1309 m) or thermal lift.
3. Gaussian Process Regression approximated the analytical model most accurately (mean MAPE 0.005%, design-point error 0.013%), with conservative prediction intervals and errors concentrated at the stall-margin switch; this demonstrates approximation fidelity, not physical validation.
4. Parasite drag and aspect ratio dominate efficiency and glide angle, wing loading and $C_{L,max}$ dominate stall speed, and release height followed by C_{D0} dominate range and endurance; the surrogate reproduces these Sobol' indices within 1e-04.
5. The results rest on numerical airfoil data and an assumed C_{D0}; no wind-tunnel or flight validation, structural assessment or stability and handling evaluation was performed.

5. SUGGESTIONS

Future work should (i) replace the assumed C_{D0} with a component drag build-up, CFD or wind-tunnel data; (ii) retrain the surrogate on such non-analytical data and test whether its calibration and speed advantage hold; (iii) add structural sizing and the load cases of CS-22 Amendment 3 [18] to close the sizing loop; (iv) assess static stability and handling qualities; and (v) use the surrogate in a multi-objective optimisation that trades stall speed against glide performance.

REFERENCES

[1] Thomas, F., 1999, *Fundamentals of Sailplane Design*, translated by Milgram, J., College Park Press, College Park, MD.

[2] Mulyanto, T. and Zulkarnain, M. F., 2019, Preliminary Design of GL-1 Sailplane Cockpit Arrangement and Control Mechanism Based on EASA CS-22 Requirements, *IOP Conf. Ser.: Mater. Sci. Eng.*, Vol. 645, No. 1, 012005, doi:10.1088/1757-899X/645/1/012005.

[3] Raymer, D. P., 2018, *Aircraft Design: A Conceptual Approach*, Ed. 6, AIAA Education Series, American Institute of Aeronautics and Astronautics, Reston, VA, doi:10.2514/4.104909.

[4] Anderson, J. D., 1999, *Aircraft Performance and Design*, McGraw-Hill, Boston.

[5] Boermans, L. M. M., 2006, Research on Sailplane Aerodynamics at Delft University of Technology, *Technical Soaring*, Vol. 30, No. 1-2, 10-12.

[6] Squires, P., 1977, Configuration Optimization of a 13-Meter-Span Sport Sailplane, *Technical Soaring*, Vol. 4, No. 3, 19-28.

[7] Brunton, S. L., Noack, B. R. and Koumoutsakos, P., 2020, Machine Learning for Fluid Mechanics, *Annu. Rev. Fluid Mech.*, Vol. 52, 477-508, doi:10.1146/annurev-fluid-010719-060214.

[8] Brunton, S. L., Kutz, J. N., Manohar, K., Aravkin, A. Y., Morgansen, K., Klemisch, J., Goebel, N., Buttrick, J., Poskin, J., Blom-Schieber, A. W., Hogan, T. and McDonald, D., 2021, Data-Driven Aerospace Engineering: Reframing the Industry with Machine Learning, *AIAA J.*, Vol. 59, No. 8, 2820-2847, doi:10.2514/1.J060131.

[9] Li, J., Du, X. and Martins, J. R. R. A., 2022, Machine Learning in Aerodynamic Shape Optimization, *Prog. Aerosp. Sci.*, Vol. 134, 100849, doi:10.1016/j.paerosci.2022.100849.

[10] Thuerey, N., Weissenow, K., Prantl, L. and Hu, X., 2020, Deep Learning Methods for Reynolds-Averaged Navier-Stokes Simulations of Airfoil Flows, *AIAA J.*, Vol. 58, No. 1, 25-36, doi:10.2514/1.J058291.

[11] Sekar, V., Jiang, Q., Shu, C. and Khoo, B. C., 2019, Fast Flow Field Prediction over Airfoils Using Deep Learning Approach, *Phys. Fluids*, Vol. 31, No. 5, 057103, doi:10.1063/1.5094943.

[12] Sharpe, P. D. and Hansman, R. J., 2025, NeuralFoil: An Airfoil Aerodynamics Analysis Tool Using Physics-Informed Machine Learning, *arXiv preprint*, arXiv:2503.16323, doi:10.48550/arXiv.2503.16323; software version 0.3.3, https://github.com/peterdsharpe/NeuralFoil.

[13] Liem, R. P., Mader, C. A. and Martins, J. R. R. A., 2015, Surrogate Models and Mixtures of Experts in Aerodynamic Performance Prediction for Aircraft Mission Analysis, *Aerosp. Sci. Technol.*, Vol. 43, 126-151, doi:10.1016/j.ast.2015.02.019.

[14] Rao, J. P. and Chimata, S. N., 2024, Machine Learning-Based Surrogates for eVTOL Performance Prediction and Design Optimization, *Metascience in Aerospace*, Vol. 1, No. 3, 246-267, doi:10.3934/mina.2024011.

[15] Tfaily, A., Bartoli, N., Diouane, Y. and Kokkolaras, M., 2026, Transfer Learning in Surrogate Modeling with Emphasis on Aircraft Design, *Struct. Multidiscip. Optim.*, Vol. 69, No. 2, 41, doi:10.1007/s00158-025-04239-w.

[16] Opgenoord, M. M. J., Allaire, D. L. and Willcox, K. E., 2016, Variance-Based Sensitivity Analysis to Support Simulation-Based Design Under Uncertainty, *J. Mech. Des.*, Vol. 138, No. 11, 111410, doi:10.1115/1.4034224.

[17] Sukmana, M. N., 2011, Preliminary Design Prestasi Terbang Pesawat Glider, *Skripsi* (unpublished undergraduate thesis, available from the authors on request), Jurusan Teknik Penerbangan, Sekolah Tinggi Teknologi Adisutjipto, Yogyakarta.

[18] European Union Aviation Safety Agency (EASA), 2021, *Certification Specifications, Acceptable Means of Compliance and Guidance Material for Sailplanes and Powered Sailplanes (CS-22)*, Amendment 3, Annex to ED Decision 2021/013/R, Cologne.

[19] Abbott, I. H. and von Doenhoff, A. E., 1959, *Theory of Wing Sections*, Dover Publications, New York.

[20] Nita, M. and Scholz, D., 2012, Estimating the Oswald Factor from Basic Aircraft Geometrical Parameters, *Proceedings of the Deutscher Luft- und Raumfahrtkongress 2012*, Berlin, September 10-12.

[21] Drela, M., 1989, XFOIL: An Analysis and Design System for Low Reynolds Number Airfoils, in Mueller, T. J. (ed.), *Low Reynolds Number Aerodynamics*, Lecture Notes in Engineering, Vol. 54, Springer, Berlin, 1-12, doi:10.1007/978-3-642-84010-4_1.

[22] McKay, M. D., Beckman, R. J. and Conover, W. J., 1979, A Comparison of Three Methods for Selecting Values of Input Variables in the Analysis of Output from a Computer Code, *Technometrics*, Vol. 21, No. 2, 239-245, doi:10.2307/1268522.

[23] Breiman, L., 2001, Random Forests, *Mach. Learn.*, Vol. 45, No. 1, 5-32, doi:10.1023/A:1010933404324.

[24] Friedman, J. H., 2001, Greedy Function Approximation: A Gradient Boosting Machine, *Ann. Stat.*, Vol. 29, No. 5, 1189-1232, doi:10.1214/aos/1013203451.

[25] Rasmussen, C. E. and Williams, C. K. I., 2006, *Gaussian Processes for Machine Learning*, MIT Press, Cambridge, MA, doi:10.7551/mitpress/3206.001.0001.

[26] Smola, A. J. and Schölkopf, B., 2004, A Tutorial on Support Vector Regression, *Stat. Comput.*, Vol. 14, No. 3, 199-222, doi:10.1023/B:STCO.0000035301.49549.88.

[27] Pedregosa, F., Varoquaux, G., Gramfort, A., Michel, V., Thirion, B., Grisel, O., Blondel, M., Prettenhofer, P., Weiss, R., Dubourg, V., Vanderplas, J., Passos, A., Cournapeau, D., Brucher, M., Perrot, M. and Duchesnay, E., 2011, Scikit-learn: Machine Learning in Python, *J. Mach. Learn. Res.*, Vol. 12, 2825-2830; software version 1.9.1, https://scikit-learn.org.

[28] Herman, J. and Usher, W., 2017, SALib: An Open-Source Python Library for Sensitivity Analysis, *J. Open Source Softw.*, Vol. 2, No. 9, 97, doi:10.21105/joss.00097; software version 1.6.0, https://github.com/SALib/SALib.

[29] Sobol', I. M., 2001, Global Sensitivity Indices for Nonlinear Mathematical Models and Their Monte Carlo Estimates, *Math. Comput. Simul.*, Vol. 55, No. 1-3, 271-280, doi:10.1016/S0378-4754(00)00270-6.

[30] Saltelli, A., Annoni, P., Azzini, I., Campolongo, F., Ratto, M. and Tarantola, S., 2010, Variance Based Sensitivity Analysis of Model Output. Design and Estimator for the Total Sensitivity Index, *Comput. Phys. Commun.*, Vol. 181, No. 2, 259-270, doi:10.1016/j.cpc.2009.09.018.

[31] Queipo, N. V., Haftka, R. T., Shyy, W., Goel, T., Vaidyanathan, R. and Tucker, P. K., 2005, Surrogate-Based Analysis and Optimization, *Prog. Aerosp. Sci.*, Vol. 41, No. 1, 1-28, doi:10.1016/j.paerosci.2005.02.001.

[32] Forrester, A. I. J., Sobester, A. and Keane, A. J., 2008, *Engineering Design via Surrogate Modelling: A Practical Guide*, Wiley, Chichester, doi:10.1002/9780470770801.